ISSN 1063-7710, Acoustical Physics, 2020, Vol. 66, No. 5, pp. 469–476. © Pleiades Publishing, Ltd., 2020.

CLASSICAL PROBLEMS OF LINEAR ACOUSTICS AND WAVE THEORY

Characterization and Optimization of Acoustic Field for Curved Array Probe

Li Lin[a], Huan-qing Cao[a], and Zhong-bing Luo[a, *]

[a] *NDT and E Laboratory, Dalian University of Technology, Dalian, 116085 China*

**e-mail: zhbluo@dlut.edu.cn*

Received September 3, 2019; revised April 23, 2020; accepted April 28, 2020

Abstract—The focusing principle and acoustic field characteristics of curved array probe are studied. Delay laws are first computed in the same way as linear array probe, and its effects on the axial acoustic pressure distributions are quantitatively examined. It is shown that the maximum points of axial acoustic pressure occur at positions deviating from the predefined focal depths. To further analyze the focusing principle of curved array probe, simulations of acoustic field are conducted under different settings of focal depth and active aperture size. It reveals that the circular array profile and the inconsistent electronic delay laws make the pulsed ultrasonic waves unable to constructively interfere at target positions. Subsidiary beams arise and further interfere with the axial acoustic pressure distributions of the main beam. To control the transmitted acoustic field, and thus customize the inspection strategy, an optimized delay law calculation scheme is proposed. The good behavior is well validated both by theoretical calculation and experimental examination.

Keywords: curved array probe, acoustic field, focusing principle, delay laws

DOI: 10.1134/S1063771020050097

1. INTRODUCTION

Components with complex surface are quite common in modern industry, like many welding joints and corner parts [1, 2]. These complex geometries do, however, bring inspection challenges [3, 4]. For conventional ultrasonic testing, inspections of complex parts are performed manually or mechanically with single element transducer to realize full coverage in the form of normal incidence. However, this point to point scanning is inefficient, and the interpretation of single A-scan exhibition is tedious and operator-dependant [5].

By contrast, ultrasonic phased array technique is able to customize characteristics of transmitted acoustic beam to improve detection and sizing capabilities for parts with complex geometries [6–8]. Among the recent advances is the arc-shaped curved array probe that ensures a normal incidence transmission of the acoustic field at any point of the surface [9]. It has been applied efficiently during engineering practice. Full coverage of the entire corner of L-shaped CFRP specimen was easily achieved through successive excitation of elements. Furthermore, the C-scan mapping views made the accurate sizing of interlaminar delamination an easy task [10, 11]. The focused acoustic field under this special array profile was investigated theoretically by some researchers. The focus law and acoustic field calculation method were presented using coordinate transformation and an approximation with rectangle element instead of circular arc element, which were further validated using Rayleigh–Sommerfeld integral and nonparaxial multi-Gaussian models, respectively [12]. Effects of main parameters, such as focal distance, steering angle, etc., on the acoustic field were also theoretically investigated by numerical simulation [13–15]. However, limited by the function of ultrasonic phased array testing equipment and for convenience, the geometrical delay law is still approximately computed in the same way as linear array probe in practice. Hence, the influences of circular array profile on the acoustic field transmitted by curved array probe were urgently needed to be quantitatively described, thus offering guidance for parameters optimization.

In this work, the effects of circular array profile on the focused acoustic field of curved array probe were investigated. Delay laws were firstly calculated in the same way as linear array, and their influences on the axial acoustic pressure distributions were quantitatively examined. An optimized delay law computation scheme was further proposed and validated.

2. RADIATED ACOUSTIC FIELD AND FOCUSING ALGORITHM OF CURVED ARRAY PROBE

The curved array probe contains a row of strip shaped elements uniformly distributed in the circumferential direction. In the Huygens' Principle

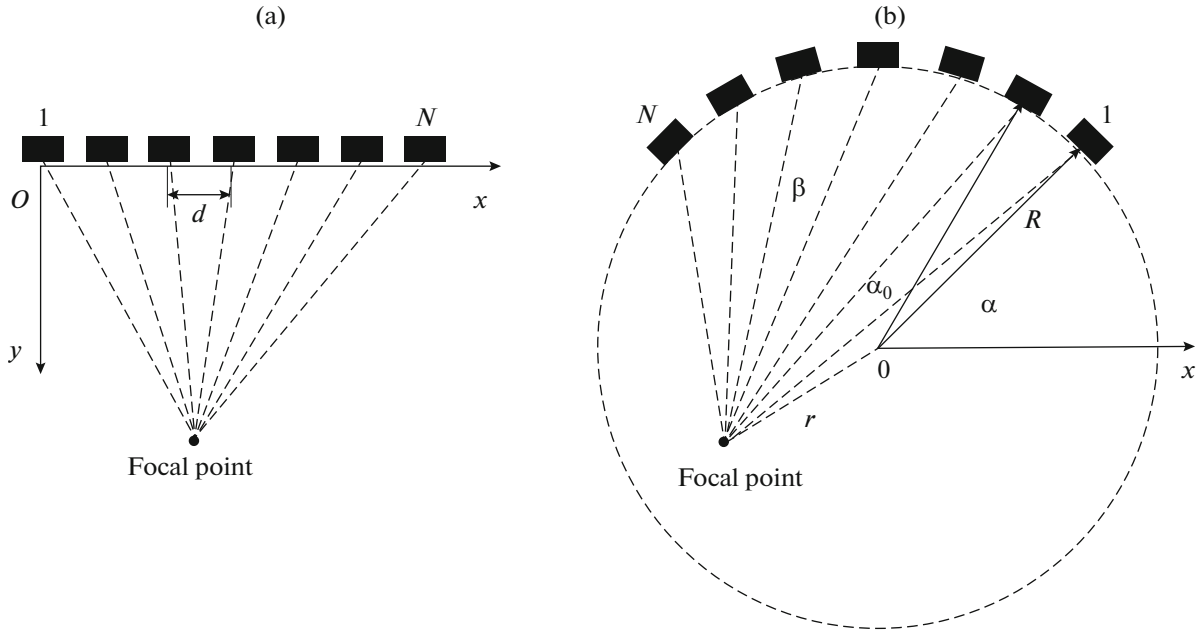

Fig. 1. Schematic diagram of delay law computation for (a)—linear and (b)—curved array probes.

approach, the acoustic pressure distribution of a transducer is described in terms of the summation of point sources representing the surface of the transducer. For a non-attenuating, homogeneous and isotropic medium with the longitudinal velocity c and the density ρ, the acoustic pressure at the field point can be calculated using the Rayleigh–Sommerfeld integral [16]:

$$p = \frac{j\rho c}{\lambda}\sum_{i=1}^{N} u_n \int_{S_n} \frac{\exp^{-jk\xi}}{\xi} dS_n, \qquad (1)$$

where j is the unit imaginary number, λ is the wavelength, S_n is the surface area of the nth element, and ξ is the distance from the point source on the nth element to the field point. Also, $u_n = U_n \exp(i(\omega t + \varphi_n))$ is the excited complex velocity of all point sources on the nth element with amplitude U_n, angular frequency ω and phase $\varphi_n = 2\pi c T_n/\lambda$, where T_n is the relative excitation time delay between elements. Obviously, for a certain array probe and acoustic medium, the relative time delay T_n is the key influential factor of the excited phase φ_n, and hence the acoustic field. This provides an effective way to control the focused ultrasonic beam.

Figure 1 shows the focusing processes of linear and curved array probes within a homogeneous and isotropic medium. The "geometrical delay law" was calculated to ensure constructive interferences at the "geometrical focusing point" defined by the focal depth and deflection angle [1]. For a linear array probe, the time of flight of ultrasonic waves from the transmitting elements to the focal point (x, y) can be calculated by the following equations:

$$T_n = \frac{1}{c}\sqrt{((n-1)d)^2 + y^2}, \qquad (2)$$

where d is the center interval between two adjacent elements for linear array probe, n (1...N) denotes the serial number of elements.

For simplicity of description, a polar coordinate was defined with origin at the center of curved array probe and horizontal polar axis. For focal point with distance r from the origin and anticlockwise angle β from polar axis, the formula of travel time of ultrasonic waves from the transmitting elements can be simplified as follows:

$$T_n = \frac{1}{c}\left(\sqrt{R^2 + r^2 - 2Rr\cos(\beta - \alpha - (n-1)\alpha_0)}\right), \qquad (3)$$

where (R, α) is the polar coordinate of the first element, α_0 is the central angle interval.

Delay laws can further be derived by substituting Eqs. (2) and (3) into the following equation:

$$\Delta T_n = \max\{T_1, T_2, \cdots, T_N\} - T_n. \qquad (4)$$

All these show that the variation of array profiles affect the delay time computation. However, for convenience, delay laws for curved array probe were still approximately computed identical to that of linear array as the curved active aperture size was small compared with the focal distance during its practical utilization. And this paper concentrates on the quantitative examination of its influence on the focused acoustic field.

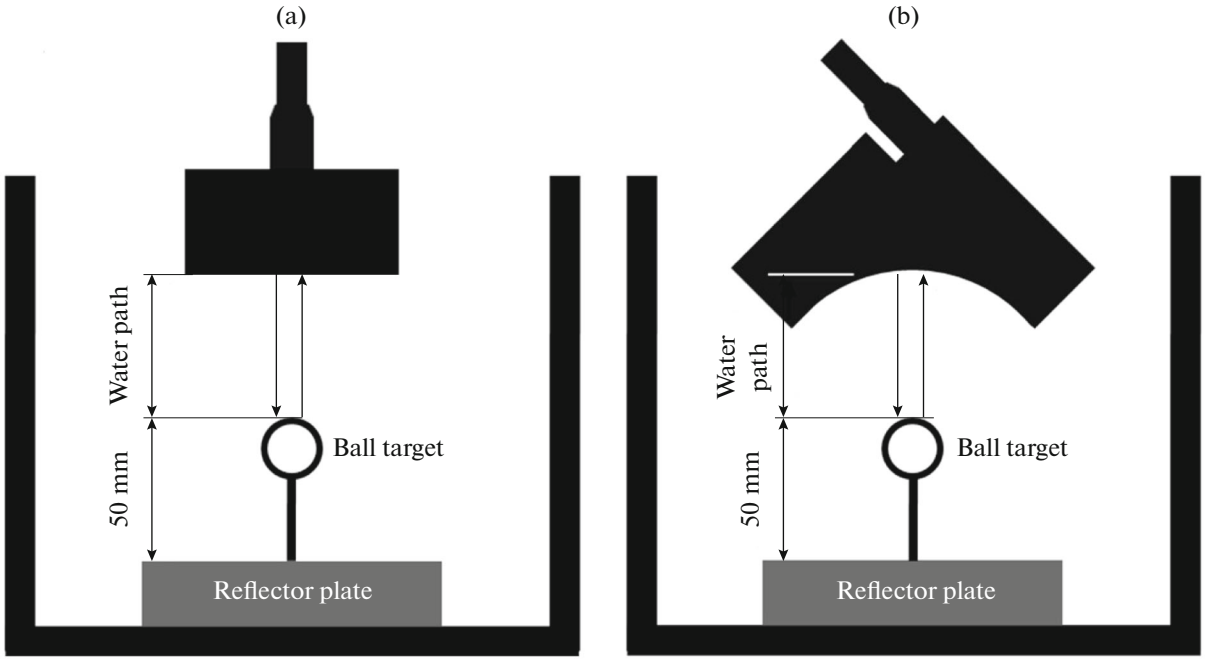

Fig. 2. Schematic diagram of experimental setup for measuring the on-axis ultrasonic beam profiles of (a)—linear and (b)—curved array probes.

3. EXPERIMENTAL MEASUREMENT OF ON-AXIS ULTRASONIC BEAM PROFILES

According to the ASTM E 1065-99 standard [17], the on-axis ultrasonic beam profiles of array probes were measured employing a pulse-echo technique using a ball target reflector, as shown in Fig. 2. A ∅6 mm smooth stainless steel ball was chosen. Probes were immersed in water and positioned over a special holder to keep the incidence direction perpendicular to the surface of reflector plate. The vertical position of probe was mechanically adjusted in a minimum step of 0.1 mm. The Olympus OmniScan MX2 flaw detector was employed to record the on-axis pressure response as a function of distance with identical transmission and reception pattern. Two types of commercial array probes were tested for comparison as listed in Table 1, where the curved array probe had a 90 degree circular surface.

Based on the phased array acoustic field theory, the effective beam focusing distance of linear array probe will be restricted within the near field length N_0 determined by the active aperture size and center frequency of pulsed ultrasonic wave, as shown in the following equation:

$$N_0 = \left(A^2 + W^2\right)\left(0.78 - 0.27W/A\right) f/\pi c, \qquad (5)$$

where A is the active aperture length (the product of No. of elements and pitch), W is the passive aperture size or element length, f is the center frequency of probe, c is the longitudinal velocity of medium [18].

Equation (5) describes the quantitative relationship between probe size and characteristics of acoustic field, and thus provides guidance for the setting of focal depth F and active aperture size during the practical applications of linear array probe. Due to the different array profiles, Eq. (5) here is used as an approximate estimation for the curved array probe. Accordingly, the calculated value of near field length under each measured condition is listed in Table 2.

Table 1. Specifications of linear and curved array probes

Array type	Center frequency, MHz	No. of elements	Pitch, mm	Elevation, mm	Radius, mm	Central angle, °
Linear	5.0	64	1.00	7.0	–	–
Curved	5.0	32	1.32	6.0	25.0	90

Table 2. Experimental measurement conditions and the estimated corresponding near field lengths

Array type	Active aperture length (No. of elements)	N_0, mm	Focal depth, mm						
			15.0	25.0	35.0	45.0	55.0	65.0	500.0
Linear	4	20.9	√	*	*	*	*	*	*
	8	65.4	√	√	√	√	√	√	*
	12	128.3	√	√	√	√	√	√	*
Curved	4	32.0	√	√	*	*	*	*	*
	8	98.6	√	√	√	√	√	√	*
	12	207.8	√	√	√	√	√	√	*

* Denotes that the value of focal depth is beyond the corresponding near field length.

4. EXPERIMENTAL RESULTS AND DISCUSSIONS

4.1. Axial Acoustic Pressure Distribution under Delay Laws of Linear Array Pattern

Figure 3 shows the on-axis acoustic pressure distribution under the condition of 8 elements active aperture for both array probes. The corresponding location of maximum points, i.e. real focal positions, were also presented. For linear array probe, as shown in Fig. 3a, the axial acoustic pressure distributions all had one single maximum point and the peak amplitude monotonically decreased when focal depth lay below 55.0 mm. Further extended the focal depth to 500.0 mm which can be regarded as focusing at infinity, the relative delay time between elements were rather tiny deduced from Eqs. (2) and (4). Thus, an approximate planar wave front was transmitted, and the axial acoustic pressure distribution presented a similar trend as the conventional single element probe, i.e. fluctuating in the near field and followed by gradually weakening in the far field (>67.7 mm). The evolution of real focal positions was also quantitatively described in Fig. 3b. Two-stage characteristic was obtained with a division point at 25.0 mm. The initial stage showed good consistency between real focal positions and predefined focal depths. However, deviation occurred when coming to the latter stage. This is not completely consistent with Eq. (5) for linear array probe.

As for the curved array probe, the axial acoustic pressure distribution still presented a distinct single-peak type, as shown in Fig. 3c, but the peak amplitude monotonically increased with focal depth even at infinity. Accordingly, the real focal positions differed from the predefined value and kept approaching to the horizontal asymptote of 25.0 mm, i.e. the circle-center of probe, as shown in Fig. 3d. Eq. (5) is still not applicable here.

The influences of active aperture size on the axial acoustic pressure distributions of linear and curved array probes were also comparatively analyzed under fixed focal depth. Here, 15.0 and 25.0 mm focal depths were chosen which were within the estimated near field lengths of all tested active apertures for linear and curved array probes, respectively. Results show that the axial acoustic pressure distributions all attained the maximum at positions close to the predefined focal depths under the condition of $A = 8 \times 1$ mm and $A = 12 \times 1$ mm for linear array probe, as shown in Fig. 4a. A 5.1 mm deviation occurred at $A = 4 \times 1$ mm, which is mainly due to the limited focusing capability of small active aperture. Meanwhile, the peak amplitude decreased with the increase of active aperture size.

As for curved array probe, the axial acoustic pressure distribution also had a major single peak trend, but none of them precisely focused at predefined focal depth with a minimum deviation of 12.4 mm. And for $A = 12 \times 1$ mm, abnormal increase of low level occurred after 18.27 mm, as shown in Fig. 4b. This implies that the acoustic waves do focused differently between linear and curved array probes.

4.2. Acoustic Simulation and Delay Law Optimization

For further analysis on the aforementioned experimental results, the CIVA 11.0 software (French Atomic Energy Commission) was used to simulate the acoustic field in water of curved array probe, which had the same specifications as described in Table 1. Two patterns of delay laws were calculated using Eqs. (2)–(4), and were applied to the simulation, respectively.

Numerical results are first presented for the acoustic field transmitted under delay laws of linear array pattern. In Figs. 5a, 5b, 5e, the two-dimensional acoustic pressure distributions are shown for varied active aperture sizes with fixed focal depth of 35.0 mm. It is shown that only 4 elements active aperture could effectively focus. Further increase in active aperture size led to the emergence of subsidiary beams on both sides of the main beam. This was mainly due to the fact that the arc-shaped active aperture of $A = 4 \times 1.32$ mm was small compared with focal depth of 35.0 mm, thus the influence of circular array profile on delay law calculation could be negligible. For larger active apertures shown in Figs. 5b, 5e, the relative delay time

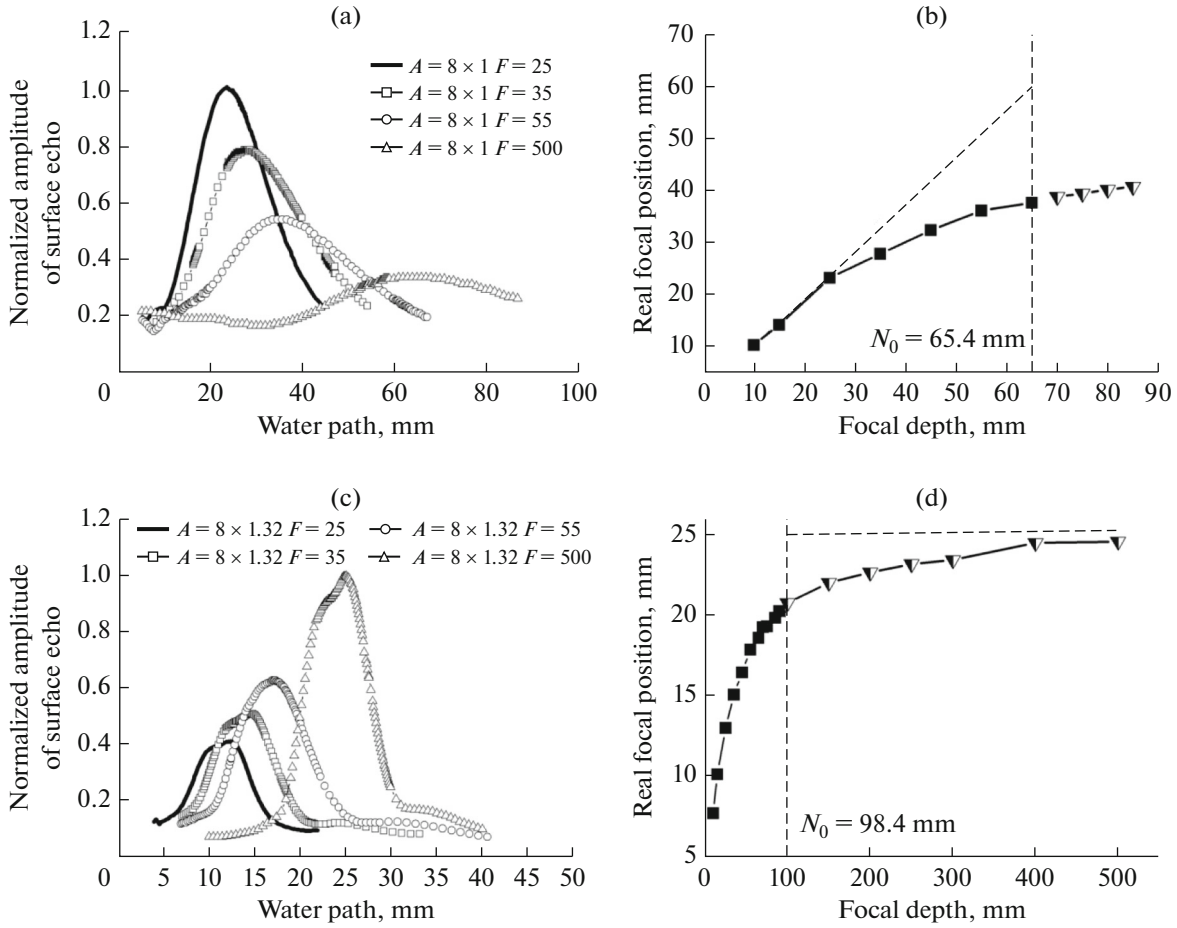

Fig. 3. Axial acoustic pressure distributions and measured focal positions for (a, b)—linear and (c, d)—curved array probes under the condition of 8 elements active aperture.

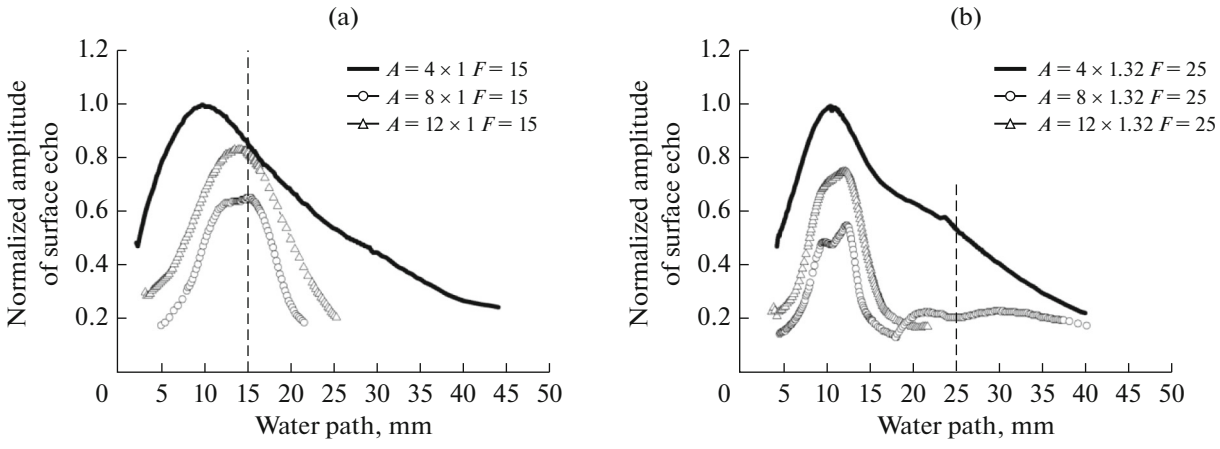

Fig. 4. Axial acoustic pressure distributions for (a)—linear and (b)—curved array probes under the condition of fixed focal depth and varied active aperture sizes.

sequence indicated by red histogram presented a convex shape. Namely, ultrasonic waves transmitted by side elements propagated to the predefined focal position prior to that of central elements, thus forming subsidiary beams beside the main beam and further caused interference. That is the reason why the axial

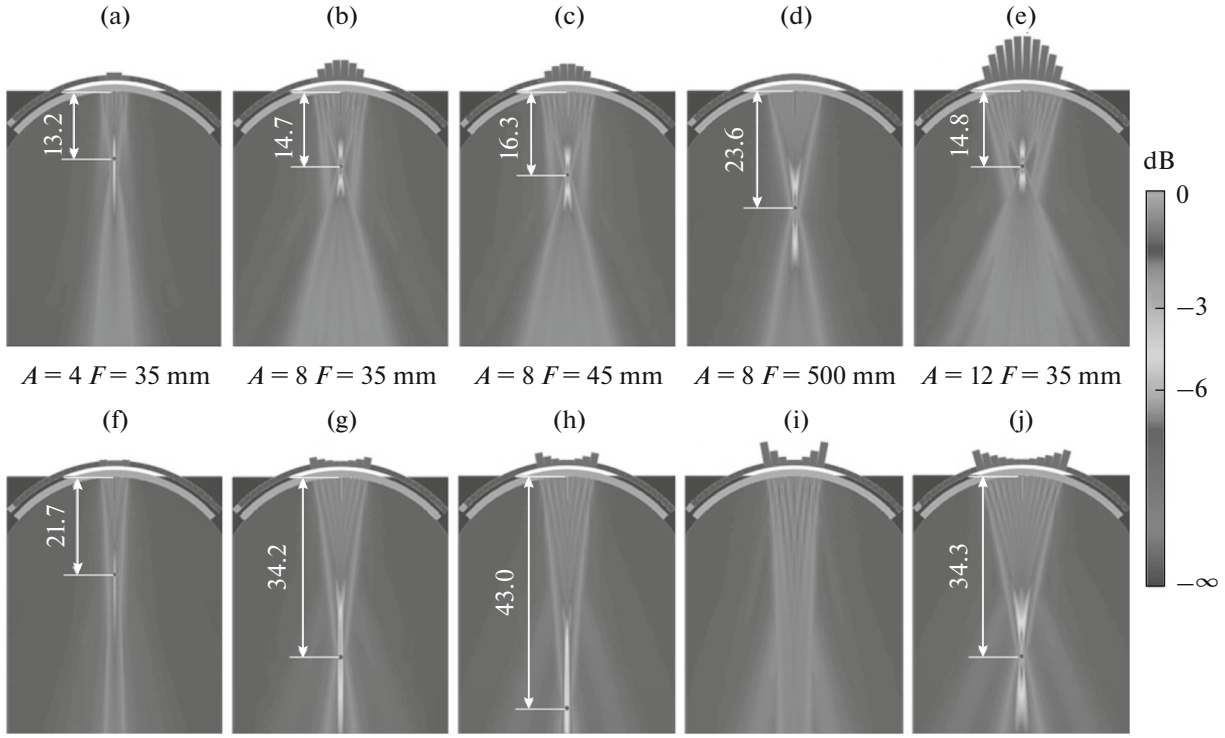

Fig. 5. Snapshots of acoustic field for curved array probe (a–e)—before and (f–j)—after delay law optimization.

acoustic pressure distribution showed abnormal increase after the peak point describe in section 4.2. This phenomenon would seriously affect the accurate interpretation of ultrasonic signals. Comparative analysis of Figs. 5b, 5c, 5d also found that the relative delay time decreased with the increase of focal depth under the condition of fixed active aperture size. Consequently, the capability of electronic focusing gradually weakened, and more ultrasonic waves naturally focused at the circle center of curved array probe. That's why the measured peak amplitude of axial acoustic pressure monotonically increased with focal depth even at infinity.

Simulation results of acoustic field transmitted under delay laws of curved array pattern are shown in Fig. 5f-j. The two-dimensional acoustic pressure distributions under all conditions were significantly optimized with one single focused acoustic beam. Contrary to the aforementioned delay laws of linear array pattern, the relative delay time of side element (1st) was 80 ns higher than that of central (4th) element under the condition of $A = 8 \times 1.32$ mm and $F =$ 35.0 mm. This concave distributed delay time sequence were able to compensate the lag between ultrasonic waves pulsed by different elements, thereby realizing constructive interference at predefined focal depth. Correspondingly, the axial acoustic pressure at 35.0 mm showed a 10.9 dB increase. In addition, the focal spot got more intensive with the increase of aperture size or the decrease of focal depth.

The simulated focal positions are shown in Fig. 6 for both patterns of delay laws. It is shown that the above features seen in the measured focal positions for the curved array probe were well reproduced by the numerical simulations conducted under delay laws of linear array pattern. In contrast, when optimize delay laws using Eqs. (3) and (4), the real focal positions showed a similar trend with that of linear array probe, which coincided well with the predefined focal depth within the range of focusing capability. The aforementioned comparative analysis revealed that to transmit a focused beam with controlled and homogeneous characteristics, the effects of circular array profile on the acoustic field distribution shall be taken into account properly in delay law computation. This is essential for the customization of inspection strategy to realize good performance.

The effectiveness of optimized delay laws were also verified by experimental measurement, and the condition of $A = 8 \times 1.32$ mm and $F = 35.0$ mm was selected for comparative analysis before and after delay law optimization, as shown in Fig. 7. The axial acoustic pressure distribution of curved array probe all possessed one single maximum point without any obvious fluctuations. When delay laws were optimized and applied under the condition of 15.0 mm fixed focal depth and varied active aperture sizes, the maximum deviation of 1.5 mm between the real focal positions and predefined focal depths appeared at $A = 12 \times 1.32$ mm. Besides, the acoustic field got sharper with the

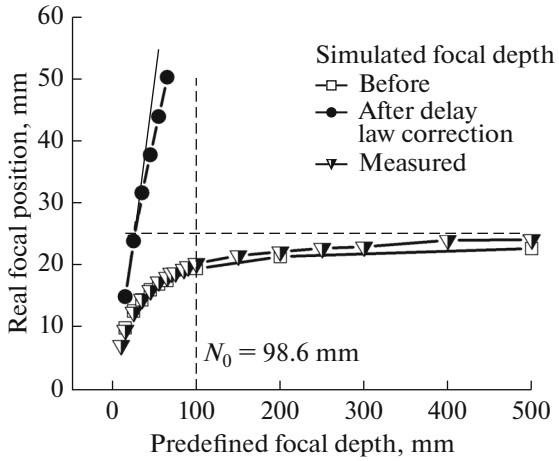

Fig. 6. Evolution of simulated focal position as a function of the predefined focal depth for curved array probe before and after delay law optimization.

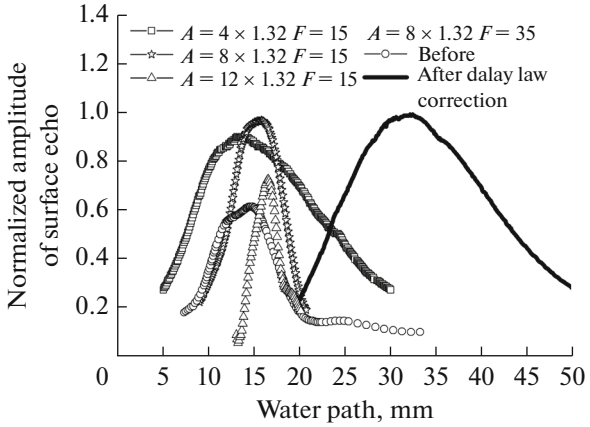

Fig. 7. Axial acoustic pressure distributions for curved array probe after delay law optimization.

increase of active aperture size. Comparative analysis of acoustic field before and after delay law optimization under the condition of $A = 8 \times 1.32$ mm and $F =$ 35.0 mm indicated that the optimization remarkably improved the maximum amplitude of acoustic field by 61.1%, and the deviation between the real focal position and the predefined focal depth decreased to −2.6 mm from 20.4 mm. These well reproduced the prediction results of numerical simulation.

5. CONCLUSIONS

Influences of circular array profile on the acoustic field of curved array probe were investigated through experimental measurements of on-axis ultrasonic beam profiles and acoustic field simulations. The main results are summarized as follows:

(1) When delay laws of linear array pattern were applied, the transmitted ultrasonic waves were unable to constructively interfere at predefined focal depth due to the effects of circular array profile. Subsidiary beams emerged beside the main beam and further caused interference. Abnormal increase of axial acoustic pressure occurred after the peak point, accordingly. In addition, the poor acoustic field distribution could be improved with the decrease of active aperture size or the increase of focal depth.

(2) The control of the transmitted focused beam characteristics of curved array probe was achieved using the optimized delay law computation scheme, which takes the circular array profile into consideration. It could compensate the lag between ultrasonic waves pulsed by different elements due to circular array profile. Effective single-spot focusing within the range of focusing capability could be achieved. And this has been verified by experiments under conditions of varied active aperture sizes and focal depths.

(3) For curved array probe, the complexity of its acoustic field lies in the coexistence of electronic and natural focusing. The regulation of relative time delays for elements offers an effective way of controlling the transmitted focused beam characteristics. This is essential for the customization of inspection strategy to fulfill the requirements of engineering applications.

FUNDING

This study was funded by the National Basic Research Program of China (grant no. 2014CB046505) and the Dalian Support Plan for Innovation of High-level Talents (Youth Science and Technology Stars, grant no. 2018RQ40).

REFERENCES

1. S. Chatillon, G. Cattiaux, M. Serre, and O. Roy, Ultrasonics **38**, 131 (2000).
2. S. Robert, O. Casula, O. Roy, and G. Neau, Meas. Sci. Technol. **24**, 074011 (2013).
3. D. Hopkins, G. Neau, and L. L. Ber, in *Proc. Workshop on Smart Materials and Structural Health Monitoring and NDT in Aerospace in Conjunction with the NDT in Canada 2011 Conf.* (Montreal, 2011).
4. N. Xu and Z. G. Zhou, NDT & E Int. **63**, 28 (2014).
5. S. V. Ramanan, A. Bulavinov, S. Pudovikov, C. Boller, and T. Wenzel, in *Proc. Int. Symp. on NDT in Aerospace* (Hamburg, 2010).
6. D. Hu, Q. Wang, K. Xiao, and Y. Ma, Procedia Eng. **43**, 459 (2012).
7. C. Frederick, A. Porter, and D. Zimmerman, in *Proc. ASME 2009 Pressure Vessels and Piping Conf.* (Prague, 2009), p. 1295.
8. P. B. Rosnitskiy, B. A. Vysokanov, L. R. Gavrilov, O. A. Sapozhnikov, and V. A. Khokhlova, IEEE Trans. Ultrason. Ferroelect. Freq. Control **65** (4), 630 (2018).
9. J. Habermehl and A. Lamarre, in *Proc. 17th World Conf. on Nondestructive Testing* (Shanghai, 2008).
10. D. M. Zhang, G. Yu, Z. G. Zhou, and N. J. B. Xu, Univ. Aeronaut. Astronaut. **39** (5), 688 (2013).

11. A. S. Boychuk, A. S. Generalov, and A. V. Stepanov, in *Proc. 12th Int. Conf. "Application of Contemporary Non-Destructive Testing in Engineering"* (Ljubljana, 2013), p. 51.
12. C. G. Xu, L. J. Wang, D. G. Xiao, and S. Y. Zhou, in *Proc. Review of Progress in Quantitative Nondestructive Evaluation* (Burlington, VT, 2011), p. 867.
13. L. L. Yu, W. D. Shou, and C. Hui, Chin. Phys. Lett. **28** (10), 104302 (2011).
14. P. B. Rosnitskiy, L. R. Gavrilov, P. V. Yuldashev, O. A. Sapozhnikov, and V. A. Khokhlova, Acoust. Phys. **63** (5), 531 (2017).
15. P. B. Rosnitskiy, P. V. Yuldashev, and V. A. Khokhlova, Acoust. Phys. **61** (3), 301 (2015).
16. F. S. Foster, M. Arditi, and J. W. Hunt, J. Acoust. Soc. Am. **68** (1), 85 (1980).
17. ASTM Committee E-7 on Nondestructive Testing, *ASTM Standard No. E 1065-99 (1999): Standard Guide for Evaluating Characteristics of Ultrasonic Search Units* (ASTM Int., West Conshohocken, 2005).
18. Olympus NDT, *Advances in Phased Array Ultrasonic Technology Application* (Olympus NDT, Waltham, 2007).